Published online 23 November 2017

Nucleic Acids Research, 2018, Vol. 46, No. 2 ***929–941***
doi: 10.1093/nar/gkx1183

Biochemical and structural characterization of a novel cooperative binding mode by Pit-1 with CATT repeats in the macrophage migration inhibitory factor promoter

Sorabh Agarwal[1] and Thomas Yoonsang Cho[1,2,*]

[1]Edward A. Doisy Department of Biochemistry and Molecular Biology, Saint Louis University School of Medicine, St. Louis, MO 63104, USA and [2]Department of Biochemistry and Biophysics, Texas A&M University, College Station, TX 77843, USA

Received August 09, 2017; Revised November 08, 2017; Editorial Decision November 09, 2017; Accepted November 14, 2017

ABSTRACT

Overexpression of the proinflammatory cytokine macrophage migration inhibitory factor (MIF) is linked to a number of autoimmune diseases and cancer. MIF production has been correlated to the number of CATT repeats in a microsatellite region upstream of the *MIF* gene. We have characterized the interaction of pituitary-specific positive transcription factor 1 (Pit-1) with a portion of the *MIF* promoter region flanking a microsatellite polymorphism (−794 $CATT_{5–8}$). Using fluorescence anisotropy, we quantified tight complex formation between Pit-1 and an oligonucleotide consisting of eight consecutive CATT repeats (8xCATT) with an apparent K_d of 35 nM. Using competition experiments we found a 23 base pair oligonucleotide with 4xCATT repeats to be the minimum DNA sequence necessary for high affinity interaction with Pit-1. The stoichiometry of the Pit-1 DNA interaction was determined to be 2:1 and binding is cooperative in nature. We subsequently structurally characterized the complex and discovered a completely novel binding mode for Pit-1 in contrast to previously described Pit-1 complex structures. The affinity of Pit-1 for the CATT target sequence was found to be highly dependent on cooperativity. This work lays the groundwork for understanding transcriptional regulation of MIF and pursuing Pit-1 as a therapeutic target to treat MIF-mediated inflammatory disorders.

INTRODUCTION

MIF plays an essential role in immune system regulation and acts as an integral component during the production of proinflammatory cytokines including TNFα, IL1β and IL-6 (1–3). However, an overproduction of proinflammatory cytokine MIF has been shown to play a role in a number of immune related pathologies, including sepsis, cancer and autoimmune diseases such as rheumatoid arthritis and inflammatory bowel disease (1,4,5). MIF expression is regulated by a number of transcription factors (Figure 1A), which have been the focus of recent research (6–8). The *MIF* gene is located on chromosome 22q11.2. The number of CATT repeats in a microsatellite sequence (−794 $CATT_{5–8}$) in the 5′-untranslated region of the *MIF* gene is correlated to both increased MIF expression and rheumatoid arthritis disease susceptibility and severity (9,10). The microsatellite sequence consists of five to eight repeats of a four-nucleotide CATT sequence. Recently Yao *et al.* identified the putative transcription factors Ubiquitin Like With PHD And Ring Finger Domains 1 (UHRF1) and Pit-1 from the nuclear extract of human THP-1 monocytes using ∼100 bp of the *MIF* promoter region encompassing this microsatellite repeat (11). In order to better understand the causes of and treatments for MIF associated diseases, we have focused on the characterization of these putative transcription factors with the *MIF* promoter region, specifically the repeating CATT element. We found that Pit-1 directly interacts with this region in a CATT dependent fashion.

Pit-1 is a 33kDa homeobox protein transcription factor that is expressed in a variety of cell types and plays a role in the production of human growth hormone, prolactin and TSHβ (12) as well as roles in immunology (13), cancer and DNA repair (14). Pit-1 has been shown to act as both an activator and repressor of gene expression (12,14). It consists of a Ser/Thr rich unstructured transactivating

*To whom correspondence should be addressed. Tel: +1 979 845 8548; Fax: +1 979 862 7638; Email: thomas.cho@tamu.edu
Present address: Sorabh Agarwal, Department of Chemistry and Chemical Biology, Northeastern University, Boston, MA 02115, USA.

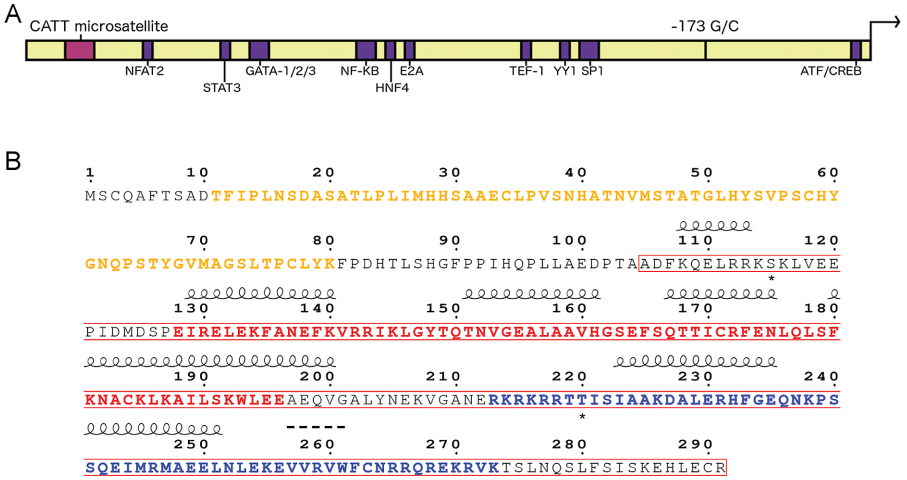

Figure 1. (**A**) The 5′-untranslated region of the *MIF* gene transcription start site is shown here. Putative transcription factor sites (in purple) were determined using MotifMap and previously identified putative sites (9,74). The −173 G/C polymorphism has been identified as a risk factor in autoimmune diseases (75,76). The −794 CATT microsatellite region consists of five to eight CATT repeats. (**B**) Secondary structure alignment predicted by PsiPred (77). Sequence boxed in red is the Pit-1$^{\Delta N}$ construct (residues 104–291) used for fluorescence anisotropy experiments. Orange lettering identifies the unstructured TAD, red lettering identifies the POU_S domain and blue lettering identifies POU_H domain. Alpha helices are denoted by loops, beta sheets by dashes and residues phosphorylated by PKA with an *. Created with ESPript (http://espript.ibcp.fr/ESPript/ESPript/) (78).

domain (TAD) that functions in transcriptional stimulation, followed by a bipartite POU domain (named after Pit1, Oct1, Oct2 and Unc86) consisting of a specific domain (POU_S) that determines sequence specificity and a homeodomain (POU_H) that contributes to DNA recognition and interaction with other transcription factors (Figure 1B) (12,15,16). This transcription factor has been shown to bind to its cognate oligonucleotide sequences and to interact with a wide variety of transcription factors in various ways using flexible yet specific mechanisms (17–19). Multimerization and interaction with other transcription factors are key factors that have been identified as affecting the outcome of gene regulation by Pit-1. Based on the sequence of the element bound, Pit-1 can bind as a monomer, a heterodimer or a homodimer (18–20). Spacing and orientation of the POU domains with respect to one another can vary unexpectedly, dependent on the sequence as illustrated by the structures of Pit-1 with the prolactin promoter (Prl-1P) and human growth hormone promoter (GH-1) DNA elements (17). Differential spacing observed in Pit-1 complexes has been identified as another critical factor conferring activation or restriction of gene expression based on cell type (17,21). Finally, phosphorylation by protein kinase A (PKA) of residues serine 115 and threonine 220 in Pit-1 has been shown to alternatively decrease, increase and have no effect on affinity for DNA, dependent on the binding sequence (22–24).

In order to understand the binding of this versatile transcription factor to the functionally significant CATT repeat region of *MIF*, we identified the minimal DNA sequence necessary for high affinity Pit-1 binding, determined the stoichiometry of the interaction and crystallized the complex. Here, we present that Pit-1 has significantly higher affinity for CATT repeats than UHRF1. Using a fluorescence anisotropy assay, we show that phosphorylation decreases the affinity of Pit-1 for the CATT repeats. Competition experiments demonstrate that at least 4 CATT repeats are necessary for high affinity interaction with Pit-1. We also determine that Pit-1 binds the 4xCATT nucleotide cooperatively in a 2:1 stoichiometry. With the insights derived from biochemical experiments, we were able to crystallize and structurally characterize the complex. The complex structure shows a significant rearrangement of POU domains relative to previously characterized Pit-1 DNA complex structures and underscores the critical role cooperativity plays in sequence recognition. This work contributes to understanding the mechanism by which the CATT region is involved in the activation of *MIF* gene expression, underscores the extraordinary variability of Pit-1 in its ability to recognize binding sites and lays the groundwork for future functional experiments for therapeutic interventions.

MATERIALS AND METHODS

Oligonucleotide synthesis

All oligonucleotides used were double-stranded and synthesized by IDT (Coralville, IA) as listed in Supplementary Table S1. All reverse complementary strands were unlabeled. 6-FAM (fluorescein) and biotin oligonucleotides were labeled on the 5' end of sense strands and purified by HPLC. DNA used in analytical sizing and crystallization experiments were also HPLC purified. Oligonucleotides were resuspended in 10 mM Tris 8.0, 1 mM EDTA and 50 mM NaCl (TE buffer), concentrations were measured in triplicate by absorbance at 260 nm. Annealing was carried out with complementary strands incubated in a 1:1 fashion in TE buffer, heated to 95°C for 3 min and cooled to 25°C.

Expression and purification of recombinant TEV and PKA

TEV protease plasmid pRK793 was a gift from David Waugh (Addgene plasmid #8827) and was purified using HisTrap resin as described (25). Briefly the TEV construct was expressed using IPTG in Rosetta2 (DE3) competent

cells and lysed in 20 mM Tris pH 8.0, 500 mM NaCl, 10% glycerol, 40 mM imidazole with 1 μg/ml of DNAse. Clarified cell lysate was run down a HisTrap column and eluted with a gradient up to 300 mM imidazole. Dialysis carried out overnight against 50 mM Tris–HCl pH 7.5, 1 mM EDTA, 5 mM DTT, 10% glycerol. Concentrated to 1 mg/ml, glycerol added to 50% and samples flash frozen and stored at −80°C. PKA plasmid was a gift from Susan Taylor (Addgene plasmid #14921) (26). PKA purification was purified on HisTrap using 50 mM Tris pH 7.8, 500 mM NaCl, 5% glycerol with 10 or 300 mM imidazole for the wash and elution buffers respectively. Protein was exchanged into 50 mM Tris–HCl pH 7.5, 0.1 mM DTT, 25% glycerol and flash frozen.

Expression and purification of recombinant UHRF1

UHRF1 in the PSG5 plasmid was a gift from Richard Bucala and the UHRF1 gene was cloned into a pET28-MHL construct using NdeI and HindIII. The final construct contains a hexahistidine tag fused to the N-terminus. The construct was expressed using IPTG in Rosetta2 (DE3) competent cells and lysed by French Press in 50 mM Tris pH 7.8, 200 mM NaCl, 10% glycerol, 0.1 mM DTT, 10 μM $ZnCl_2$ (Buffer A) with 10 mM imidazole, 0.25 mg/ml lysozyme, 5 ug/ml leupeptin, 15 μg/ml benzamidine, 1 ug/ml pepstatin and 1 mM PMSF. Clarified cell lysate was run down a HisTrap column with Buffer A containing 10 and 300 mM imidazole used as wash and elution buffers respectively. Sample was concentrated to approximately 3 mg/ml and the 1:30 TEV was added by mass and sample was dialyzed overnight against Buffer A. Half the sample was used for PKA phosphorylation (see below). Samples were subsequently cleaned up by reinjection on HisTrap resin. Protein was exchanged into Buffer A with 30% glycerol and 0.5 mM DTT, concentrated to 1 mg/ml, flash frozen and stored at −80°C.

Expression and purification of recombinant Pit-1

Pit-1 in pENTR223.1 was a gift from The ORFeome Collaboration (DNASU plasmid #83098) (27). The portion of the Pit-1 gene desired was cloned into a pET28-MHL construct using NdeI and HindIII. Pit-1^{wt} included residues 1 to 291, Pit-$1^{\Delta N}$ residues 105–291 and Pit-$1^{\Delta N \Delta C}$ residues 124–273. The final construct contains a hexahistidine tag fused to the N-terminus. The construct was expressed using IPTG in Rosetta2 (DE3) competent cells and lysed by sonication in 50 mM HEPES pH 6.5, 300 mM NaCl, 10% glycerol, 0.1 mM DTT, 10 mM imidazole (buffer B) with 0.25 mg/ml lysozyme, 5 ug/ml leupeptin, 15 ug/ml benzamidine, 1 ug/ml pepstatin, 1 mM PMSF, 5 ug/ml RNase and 10 ug/ml DNase. The insoluble pellet was isolated by centrifugation at 30 000g for 45 minu. Pellets were washed with buffer B + 0.5% triton X-100, the pellet was isolated by centrifugation at 30 000g. The pellet was homogenized in 20 mM HEPES 6.5, 0.1 mM DTT, 8 M urea, 0.3 M NaCl and 20 mM Imidazole (buffer C). The soluble fraction was isolated after centrifugation at 30 000g. The urea-solubilized fraction was purified using HisTrap resin with wash, high salt wash and elution buffers consisting of buffer C, buffer C with 1.3 M NaCl and buffer C with 300 mM imidazole respectively. Pit-1 was concentrated to ∼2 mg/ml and dialyzed overnight against 20 mM HEPES 7.0, 0.3M NaCl, 0.5M sucrose, 0.5M L-arg and 0.1 mM DTT (Buffer R). A couple hours into the dialysis, a 1:30 ratio of TEV was added by mass. If necessary, half the sample was used for PKA phosphorylation (see below). Samples were subsequently cleaned up by reinjection on HisTrap resin. Protein was exchanged into Buffer R with 30% sucrose and 0.5 mM DTT, concentrated to ∼1 mg/ml, flash frozen and stored at −80°C.

PKA phosphorylation

Sample for PKA phosphorylation had 10 mM $MgCl_2$ added to it. An approximate 1:10 mass ratio of PKA:target is added. ATP is added so that final ATP concentration becomes 500 μM. Reaction is incubated at 30°C for approximately an hour during which aliquots are taken at various time points and quenched in SDS-PAGE buffer. This sample is subsequently injected onto Ni-NTA to clean up the reaction as described above. Equal volumes of time course samples were loaded onto SDS-PAGE and transferred to PVDF (GE Healthcare Life Sciences). The blots were probed with rabbit anti-phospho-PKA substrate (Cell Signaling, #9624; 1:2000), as the primary antibody. Horseradish peroxidase conjugated goat anti-IgG (Abcam, #ab97051; 1:5000) was used as the secondary antibody. Western blot band intensities were quantified using ImageJ software (NIH).

Electrophoretic mobility shift assays

TAE gels with 7% polyacrylamide (acrylamide:bis-acrylamide = 37.5:1), and 30% triethylene glycol were poured (28). Gels were run as previously described (29). Briefly, 1xTAE buffer was used with 1 mM thioglycolic acid. Gels were pre-run at 150 V for 20 min using 5 μl of pre-run buffer with triethylene glycol. Binding reactions were prepared during pre-run. Reactions were prepared in 10 mM Tris 7.4, 50 mM KCl, 5 mM $MgCl_2$, 5% glycerol, 0.05% NP-40, 0.1 mg/ml BSA, biotin labeled 111 bp 8xCATT sequence was added to 500 pM for UHRF1 reactions and 200 pM for Pit-1 reactions. Non-protein components were mixed and brought to room temperature before adding the protein. Serial dilution of the target protein was made in buffer R and added as 10× samples to reactions for a final concentration as labeled. Samples were allowed to equilibrate for ∼1/2 h at room temperature, 3 μl of 25% Ficoll was added to quench each tube and samples were loaded for EMSA. After the run, samples were transferred to nylon membrane and cross-linked using a CL-1000 UV cross-linker (UVP) for 1 minute. The blots were developed using the LightShift Chemiluminescent EMSA kit (Thermo Scientific).

Microscale thermophoresis

FAM labeled 111 bp 8xCATT or 0xCATT nucleotide was kept at a constant concentration of 200 pM for these experiments. UHRF1 was serial diluted in from 50 μM to

97.7 nM for f8x 111 and from 25 μM to 48.8 nM for f0x. The assay was performed in 10 mM Tris 7.4, 50 mM KCl, 5 mM $MgCl_2$ and 5% glycerol. After a short incubation the samples were loaded into glass capillaries and analysis was performed using the Monolith NT.115 (NanoTemper Technologies).

Fluorescence anisotropy

Fluorescence anisotropy experiments were carried out using a Spectramax i3 plate reader (Molecular Devices) with the plate incubated at 4°C prior to reads. For initial binding isotherms (Figure 2), FAM labeled oligonucleotides were used at a final concentration of 1 nM. Reactions were carried out in 10 mM Tris 7.4, 50 mM KCl, 5 mM $MgCl_2$ and 5% glycerol (Bind buffer) with an additional 5% glycerol and 0.5 mM DTT added. In all cases, blank samples consisted of all constituents in absence of FAM-labeled oligonucleotide and perpendicular and parallel polarization values were subtracted as appropriate. Serial dilutions of various Pit-1 constructs ranged from 1 μM to 0.977 nM. Data was fit using a standard four-parameter logistic fit (Prism) (30). To minimize the effect of nonspecific binding on fitting the curves, f8x curves were truncated at concentrations where the fGC and fGC79 oligonucleotides exceeded ∼30% of the anisotropy and fits were weighted by 1/X (31). Competition experiments were carried out with 1 nM f8x as the probe and 30 nM of Pit-$1^{\Delta N}$. Serial dilutions of oligonucleotide as indicated, ranged from 0.244 nM to 4 μM. When determining stoichiometries, FAM labeled DNA constructs were held at 250 nM (∼10 times the K_d of the interaction between the 4xCATT and Pit-$1^{\Delta N}$) while titrating partial molar equivalents into the reaction similar to experiments previously carried out (32,33).

Gel filtration experiments

Binding reactions were prepared and run in Bind buffer with 0.5 mM tris(2-carboxyethyl)phosphine (TCEP) and injected onto a Superdex 200 10/300 GL (GE Healthcare Life Sciences) gel filtration column at 4°C. 4xCATT nucleotide was used at a final concentration of 22.56 μM. Pit-1 was added to 22.56 μM or 45.12 μM as appropriate. For independent DNA and protein injections, appropriate volumes of Buffer R or TE buffer were added respectively. In order to determine apparent molecular weights, the column was calibrated with gel filtration standards (Bio-Rad) and the void volume determined using blue dextran.

Crystallization, data collection and structural characterization of the complex

Two protein constructs (Pit-$1^{\Delta N}$ and Pit-$1^{\Delta N\Delta C}$) as well as DNA with varying lengths and ends (blunt end, single T/A overhang and double TT/AA overhang) were screened for crystallization. Differing combinations were validated for binding activity on analytical gel filtration columns before trays were set up. Pit-$1^{\Delta N}$:4xCATT or Pit-$1^{\Delta N\Delta C}$:4xCATT was incubated at a 1.95:1 ratio, and complex was exchanged into Bind buffer with 0.5 mM TCEP added. Trays were set up with ∼6 mg/ml protein. The highest resolution diffracting crystals were obtained from a 4xCATT oligonucleotide with a single T/A overhang. Drops were set up in a ratio of 2:1 protein to precipitant (0.1 M MES pH 6.5 17.5% (w/v) PEG 6000 5% (v/v) MPD). Crystals were harvested after approximately 2 weeks at 18°C. Crystals were cryoprotected in a solution identical to the reservoir solution but containing 25% glycerol prior to flash freezing. X-ray diffraction data were collected on an inhouse Rigaku 1.2 kW MicroMax-007HF generator and Rigaku Raxis IV++ detector. Data was indexed and integrated using MOSFLM (34) followed by merging three different datasets of the same crystal at varying resolution into a single dataset using BLEND (CCP4i suite) (35,36). The data were scaled and merged using POINTLESS, AIMLESS and CTRUNCATE (37,38). The structure was solved by molecular replacement using Phaser and associated software in the PHENIX package (39). A partial molecular replacement solution was obtained with the Prl-1P complex (PDB 1AU7), and missing domains were placed manually into unfit density, MolProbity (40) was used to validate the structure. Structural figures were generated using PyMOL (41). Software used in this project was curated by SBGrid (42). The nucleotide-residue contact map was obtained by analysis of the final structure using DNAproDB (43).

RESULTS

Pit-1 is the direct CATT repeat element binder

We tested UHRF1 and Pit-1 for their ability to directly interact with the microsatellite region using the 8xCATT sequence. The 8xCATT sequence was found to pull down the most UHRF1, relative to nucleotides containing fewer CATT repeats (11). Yao *et al.* found that in absence of the CATT repeats, binding of UHRF1 and Pit-1 was abrogated indicating a specific interaction with the CATT repeats. UHRF1 and Pit-1 have been characterized as having PKA dependent binding activities (22,44). In order to determine how the initially identified putative targets UHRF1 and Pit-1 interacted with the CATT repeat region, we recombinantly expressed, purified and post translationally modified each protein with PKA (supplementary Figure S1). A 5′-biotinylated 111bp sequence in the *MIF* promoter region from −825 to −794 (including eight CATT repeats) was initially used as a probe for electrophoretic mobility shift assays (EMSA) and the same probe with a FAM label in place of biotin was used for microscale thermophoresis (MST). These initial experiments indicated that UHRF1 interacted with weak affinity (K_d > 1 μM) and that phosphorylation of UHRF1 by PKA had no significant effect (Supplementary Figures S2 and S3). In contrast, we found that both the phosphorylated and non-phosphorylated Pit-1 showed strong affinity for the 8xCATT repeat region. While not quantitated, based on the shifts one can estimate the K_d value of Pit-1 to be in the low nanomolar range, with significantly stronger binding than was present for UHRF1. We subsequently targeted this interaction for more quantitative characterization by fluorescence anisotropy.

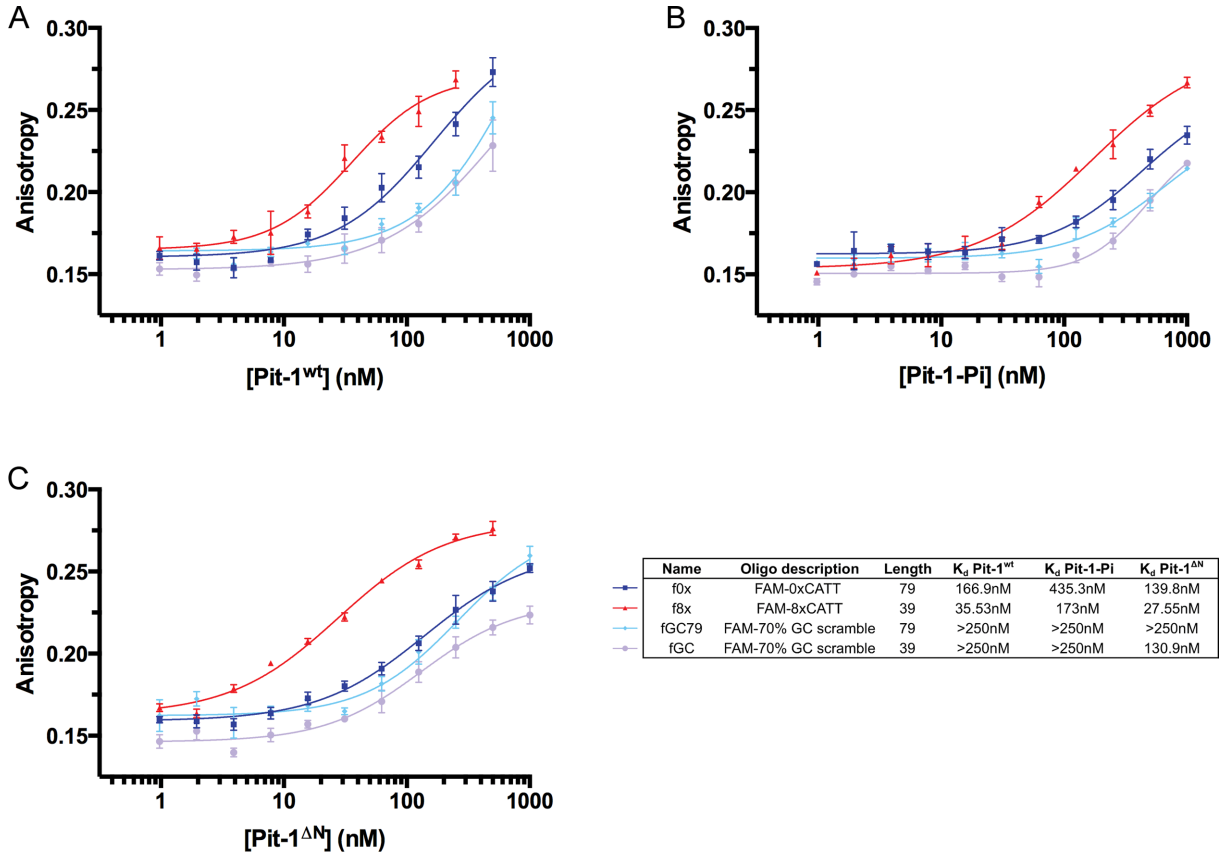

Name	Oligo description	Length	K_d Pit-1^{wt}	K_d Pit-1-Pi	K_d Pit-1$^{\Delta N}$
f0x	FAM-0xCATT	79	166.9nM	435.3nM	139.8nM
f8x	FAM-8xCATT	39	35.53nM	173nM	27.55nM
fGC79	FAM-70% GC scramble	79	>250nM	>250nM	>250nM
fGC	FAM-70% GC scramble	39	>250nM	>250nM	130.9nM

Figure 2. Binding isotherms for various Pit-1 constructs and FAM labeled oligonucleotides f0x, f8x, fGC79 and fGC. The table/key compiles K_d values from the binding isotherms discussed. (**A**) Pit-1^{wt} shows a K_d of 35 nM for f8x. f0x with DNA flanking the 8xCATT region was tested for affinity and showed a weaker K_d of 166.9 nM. 70% GC scramble oligonucleotides fGC79 and fGC showed weaker affinity with K_d values greater than 250 nM. (**B**) Pit-1-Pi shows weaker affinity than Pit-1^{wt} for every oligonucleotide tested. (**C**) Relative to Pit-1^{wt}, Pit-1$^{\Delta N}$ shows a stronger affinity for f8x and a weaker affinity for f0x. Error bars in (A–C) represent S.D. for mean from triplicate samples.

Pit-1 binds to the 8xCATT oligonucleotide with a low nanomolar affinity

In order to understand how Pit-1 interacts with the CATT region, we first characterized the interaction of the wild-type, phosphorylated and N-terminally truncated variants of Pit-1 with various FAM labeled sequences. As binding affinity of UHRF1 and Pit-1 appear to correlate to the number of repeats, we used a 39bp FAM labeled sequence with eight CATT repeats (f8x) as a probe. We also used a sequence that consisted of the DNA sequence flanking the CATT repeat (f0x), in order to establish a lack of binding sites in the flanking regions and show specificity for the CATT region.

The binding isotherms obtained by fluorescence anisotropy confirmed that Pit-1 interacted with the 8xCATT region with high affinity. We found that Pit-1^{wt} preferentially interacted with f8x compared to f0x (Figure 2A). This result indicates that the interaction identified by EMSA is primarily mediated by the CATT repeats. The K_d of this interaction with the 8xCATT sequence was determined to be 35 nM, which is consistent with previously determined K_d values of Pit-1 with specific regulatory sequences (22,45). Pit-1 is known to adventitiously interact with AT-rich regions and this may be the source of the affinity of Pit-1 for the f0x flanking sequence. To confirm this hypothesis and to characterize the effect of aggregation and nonspecific binding, we also tested two different 70% GC scrambled oligonucleotides, 39 bp long fGC and 79 bp long fGC79. These negative control sequences showed virtually identical behavior to one another, demonstrating that the difference in sequence length between f8x and f0x was not the source of the divergent affinities. We found that the affinity of fGC and fGC79 was less than that of f0x confirming GC rich sequences show weaker binding. The increased anisotropy of the f0x, fGC and fGC79 samples at higher Pit-1 concentrations is due, in part, to non-specific binding and aggregation. We subsequently used FAM labeled oligonucleotides to test the effect of phosphorylation on Pit-1 (Figure 2B) and found a significant reduction in affinity for all sequences tested, particularly for the f8x oligonucleotide. We subsequently focused on the interaction of unphosphorylated Pit-1 with CATT repeat element.

Working with Pit-1^{wt} in anisotropy assays was challenging given its inherent propensity for aggregation. The unstructured N-terminal region (residues 1–104) was truncated resulting in Pit-1$^{\Delta N}$ (Figure 1B) and carried out anisotropy assays. We found that the K_d of f8x was decreased to 27 nM and the K_d for f0x was increased, thus

improving selectivity (Figure 2C). Variation in the absolute anisotropy of the plateaus of f8x, f0x, fGC and fGC79 is due to small differences in temperature and had negligible effect on K_d values. Qualitatively, EMSA seems to suggest smaller K_d values than anisotropy experiments for characterized interactions. This discrepancy is due to the well-known 'caging effect', where K_d values are artificially decreased as a result of the gel preventing diffusion (46). For subsequent anisotropy experiments, we used Pit-$1^{\Delta N}$ as it is more CATT selective and stable under the conditions tested.

Four CATT repeats are the minimal requirement for high affinity Pit-1 binding

Having identified a truncated stable binding construct of Pit-1 that maintained its preferential affinity for the CATT repeat region, we next investigated how the number of CATT repeats affected binding of Pit-1. Competition assays were carried out using f8x as a probe and Pit$1^{\Delta N}$ as the receptor. Pit-$1^{\Delta N}$ was used at 30 nM, greater than the K_d value so that >50% of the probe was bound (47). Sequences with clearly anticipated behavior were used as competitors to verify the fidelity of the assay (Figure 3A). Two variants of the 8xCATT sequence were used: u8x 111 is the unlabeled full 111 bp 8xCATT nucleotide used in initial copurification assays (11), and u8x is a 39 bp 8xCATT sequence identical to the probe but lacking the FAM group. IC_{50} values and competition curves for u8x 111, u8x and u5x 99 were virtually identical with IC_{50} values confirming that the CATT repeats are responsible for the affinity of Pit-1. As a negative control, we assayed a 70% GC scramble sequence uGC that showed the expected poor competition. Finally, as a positive control, we used a 70 bp of the human growth hormone sequence uhGH, previously characterized to interact with a K_d of ∼20 nM by surface plasmon resonance (45). Our results for uhGH show an IC_{50} value similar to that of u8x indicating that the affinity is similar to that of 8xCATT (which was determined to be 27 nM). Due to the complexity of anisotropy assays, we were unable to make IC_{50} to K_i conversions using the Cheng–Prusoff equation (48). Despite this limitation, the IC_{50} values still allowed us to determine a rank order of affinity for the competing oligonucleotides.

Next, we quantified the interaction of Pit-1 with oligonucleotides containing varying numbers of CATT repeats to gain insight into how differing numbers of repeats affected affinity. As expected, sequences with fewer repeats of the CATT element showed a weaker ability to compete with the f8x probe for the Pit-$1^{\Delta N}$ binding site (Figure 3B). If the CATT repeat is the binding site for Pit-1 binding, then an 8xCATT strand has eight times the binding sites compared to a 1xCATT oligonucleotide. To understand this effect, we normalized the x-axis by the putative binding element for Pit-1, the concentration of CATT repeats (Supplementary Figure S4). When scaled, sequences with four or greater repeats showed highly similar IC_{50} values and curves. For IC_{50} values (both scaled and unscaled), there is a major increase in IC_{50} between the 4xCATT and 3xCATT sequences with fewer repeats leading to more poorly competing oligonucleotides (Figure 3B). This indicates a significant difference in binding mechanism. Thus, for subsequent experiments, we targeted the 4xCATT sequence. This offered several benefits: less sample heterogeneity, higher quality anisotropy data and lower mass and concentration requirements for subsequent experiments.

Pit-1 and the 4xCATT repeat oligonucleotide interact in a 2:1 ratio

We subsequently investigated the stoichiometry of the interaction between Pit-$1^{\Delta N}$ and the CATT repeat element. Titrating increasing molar equivalents of Pit-$1^{\Delta N}$ led to a plateau for the 4xCATT at 2.49 equivalents (Figure 4A). Titration of the 70% GC scramble shows a slightly positive slope likely reflecting increasing adventitious interactions and aggregation at higher protein concentrations. Unexpectedly, the 3xCATT nucleotide shows a plateau at 2.38 equivalents. Considering the final anisotropy of each plateau clarified the cause of the unexpected behavior. As shown in Figure 4A, the plateau of the f3x sequence is higher than that of the f4x sequence, indicating that the final complex formed by f4x is smaller (and thus faster rotating) than that formed by the f3x complex. This is unexpected as the DNA sequence of f3x is shorter than f4x. We speculate that one Pit-1 molecule fully binds while only a portion of the bipartite DNA binding domain of the second molecule of Pit-1 (either POU_S or POU_H) binds, leading to a less structured (and slower rotating) complex. This also explains the weaker affinity of the 3xCATT compared to the 4xCATT nucleotide. The 2.49 equivalents identified with f4x is likely the result of a combination of not all of the Pit-$1^{\Delta N}$ being active, the propensity for Pit-1 to aggregate, and nonspecific binding (33,47). This result indicates that the molar ratio of Pit-$1^{\Delta N}$ to 4xCATT is 2:1.

To confirm the interaction of two Pit-$1^{\Delta N}$ molecules with each 4xCATT DNA, we carried out gel filtration with Pit-$1^{\Delta N}$ and the 4xCATT sequence at 1:1 and 2:1 molar equivalents (Figure 4B). Absorbance was measured at 260 nm, with the protein showing little absorbance. This approach allowed us to see the effect of Pit-$1^{\Delta N}$ binding on DNA. We found that the Pit-$1^{\Delta N}$ and DNA injected independently migrated at their expected molecular weights (black and green respectively). The DNA molecule migrated at higher than its molecular weight, likely due to its elongated shape. Injection of a 1:1 ratio of Pit-$1^{\Delta N}$ to 4xCATT, showed 2 peaks: peak #1 (smaller retention volume) with an approximate apparent molecular weight of two Pit-$1^{\Delta N}$ molecules to one 4xCATT nucleotide and peak #2 (larger retention volume) with an apparent molecular weight identical to the unbound DNA. Injection of a 2:1 ratio resulted in a single peak with an approximate apparent molecular weight of two Pit-$1^{\Delta N}$ molecules to 1 4xCATT nucleotide. Injection of a 4:1 ratio resulted in an identical trace to the 2:1 ratio (not shown) indicating that additional Pit-1 molecules beyond a 2:1 ratio are unable to bind and effect DNA migration. These results confirm that the ratio of Pit-$1^{\Delta N}$ to 4xCATT is 2:1. In the intermediate case of the injection of a 1:1 ratio, DNA is present in two states, a fully complexed state (two Pit-$1^{\Delta N}$ complexed to each oligonucleotide) and free unbound DNA. This indicates that binding of Pit-$1^{\Delta N}$ is cooperative in nature. In the case of non-cooperative or uncoopera-

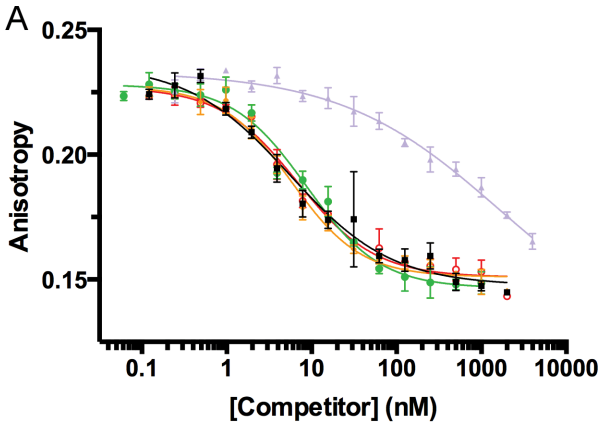

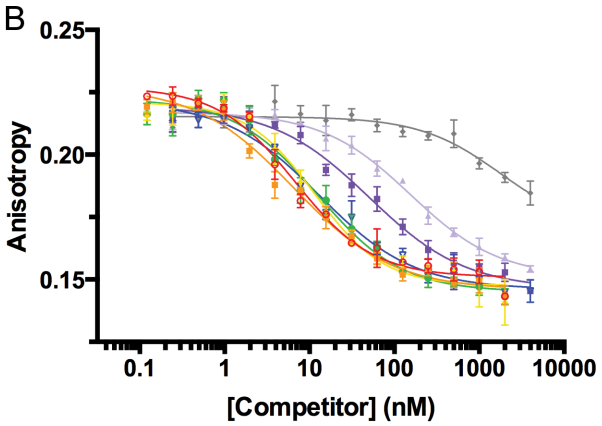

Name	Oligo description	Length	IC_{50} [Competitor]
u8x111	8xCATT	111	5.563nM
u8x	8xCATT	39	6.81nM
u5x99	5xCATT	99	5.778nM
uGC	70% GC scramble	39	1643nM
uhGH	hGH	70	8.694nM

Name	Oligo description	Length	IC_{50} [Competitor]	IC_{50} [CATT]
u8x	8xCATT	39	6.810nM	54.48nM
u7x	7xCATT	35	6.560nM	45.92nM
u6x	6xCATT	31	11.52nM	69.14nM
u5x	5xCATT	27	12.55nM	62.75nM
u4x	4xCATT	23	13.04nM	52.16nM
u3x	3xCATT	19	50.91nM	152.7nM
u2x	2xCATT	15	154.4nM	308.9nM
u1x	1xCATT	11	1814nM	1814nM

Figure 3. Competition experiments were carried out using f8x as a probe. Competing unlabeled oligonucleotides were added as described. (**A**) Control oligonucleotides were used to initially characterize the system and confirm the predictive value of competition experiments, IC_{50} values showed the expected results. (**B**) Oligonucleotides with various lengths of CATT repeats were tested for their ability to compete with f8x. Based on IC_{50} values, oligonucleotides with fewer than four CATT repeats showed significantly poorer competition behavior. The table of IC_{50} values is reported as a function of [Competitor] or [CATT]. Error bars in (A) and (B) represent S.D. for mean from triplicate samples.

tive binding we would have expected to see a population of singly bound oligonucleotide. The height of the two peaks in the 1:1 injection were almost identical, with the complex peak being smaller than that of the free DNA, supporting the anisotropy results.

Structure of Pit-1$^{\Delta N\Delta C}$ and the 4xCATT sequence

Given the lack of identity of the CATT repeat sequence to previously characterized sequences (Prl-1P and GH-1) we crystallized a complex between Pit-1$^{\Delta N\Delta C}$ and the 4xCATT nucleotide. Anisotropy experiments assisted in the design of oligonucletodies to target for crystallization, knowledge of the stoichiometry allowed us to target a 1.95:1 ratio of protein to DNA. Due to the propensity for Pit-1$^{\Delta N}$ to aggregate, Pit-1$^{\Delta N\Delta C}$ (residues 124–273) previously targeted by structural studies with Prl-1 and GH-1 was used for crystallization (17,49). Gel filtration of Pit-1$^{\Delta N\Delta C}$ with all DNA crystallographic variants screened showed identical cooperative behavior as previously discussed (not shown). A nucleotide with unpaired complementary 5′ T/A nucleotide overhang on each end (f4xCrystFI/f4xCrystRC) crystallized successfully. The complex formed rod like crystals with diffraction patterns showing clear meridional reflections at ∼3.3 Å (Supplementary Figure S5), verifying the presence of DNA (50,51). Molecular replacement was used to solve the structure, DNA bases were removed and purines and pyrimidines were identified in unbiased maps. The final unpaired nucleotides on each strand showed significant conformational dislocation thus confirming the correct modeling of the DNA molecules. Refinement was carried out with a final R-work/R-free of 23.04%/27.73% (Supplementary Table S2). Linker residues between the POU_S and POU_H domains were not observable, however based on distance measurements, the only allowable conformation was modeled (Supplementary Figure S6).

The structure of Pit-1 with the 4xCATT sequence shows 2 monomers (chain A in salmon and chain B in teal) bound to a single 4xCATT oligonucleotide as expected (Supplementary Figure S7). However, the orientation of the bound domains differs significantly from the only other Pit-1 structure in the PDB, Prl-1P (Figure 5A). Each chain consists of a POU_S followed by a POU_H domain. Overlaying the Prl-1P and 4xCATT complex structures results in nearly perfect overlap of the POU_{H2} domains from each structure and unexpectedly the POU_{S2} from 4xCATT with POU_{S1} from Prl-1P. The alternate conformations of chain B in the 4xCATT and Prl-1P structures are reminiscent of a domain swap. The remaining domains in the 4xCATT structure POH_{H1} and POU_{S1}, making up chain A, show no overlap with domains from the Prl-1P mutant structure. Chain A binds the same oligonucleotide sequence as chain B with the domains of both chains binding in the same conformation. As a consequence, the 4xCATT domain arrangement is strikingly different from the previously characterized Prl-1P and GH-1 sequences (Figure 5B). The 4xCATT sequence causes Pit-1 to adopt a novel binding mode with a significantly smaller site for each monomer, encompassed by 2xCATT repeats. In the 4xCATT complex structure, the POU_H domains are placed much more closely together with the domains oriented in different directions when compared to previous structures. As a result, the binding surface formed by the Pit-1 dimer is significantly changed.

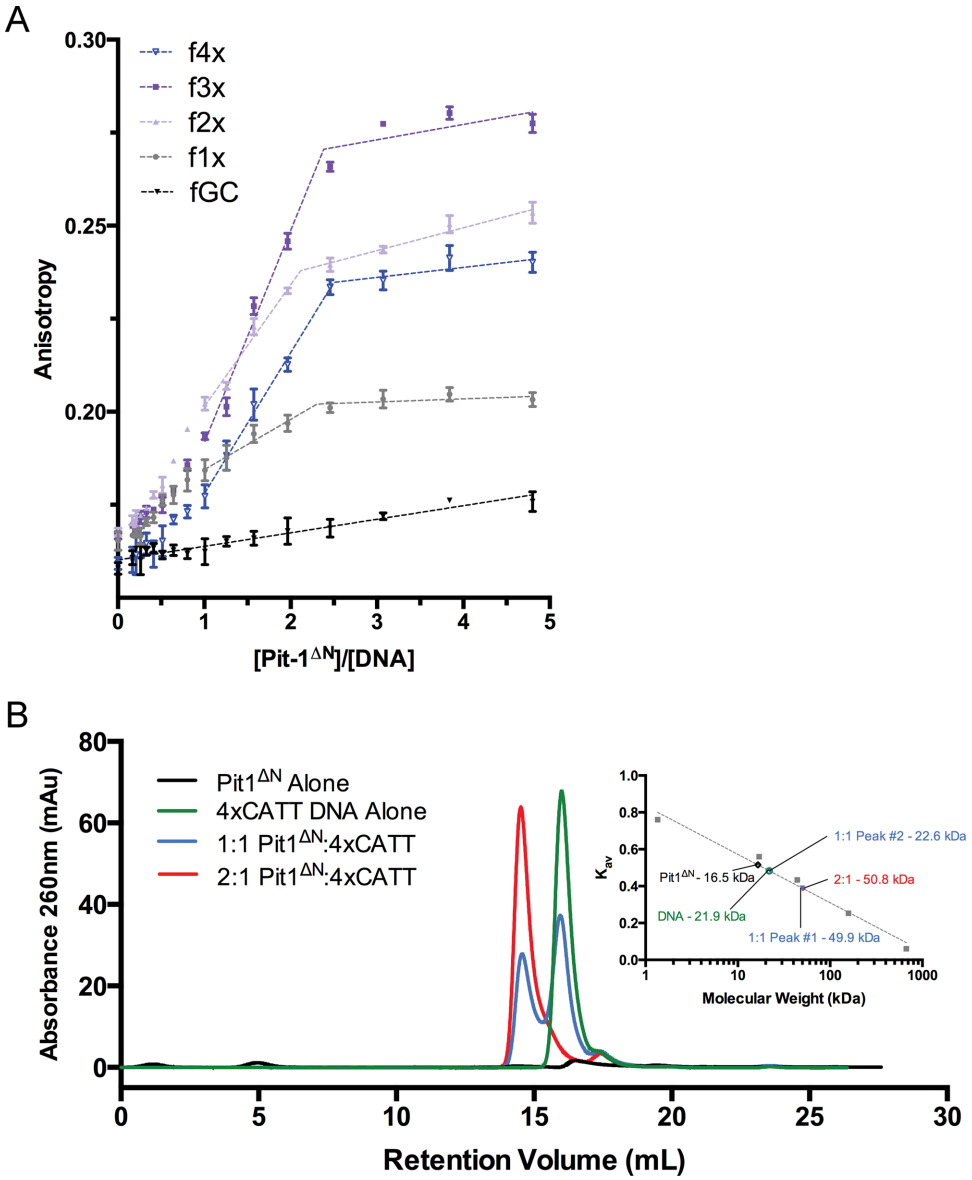

Figure 4. Anisotropy and gel filtration were used to establish the molarity of the interaction of Pit-1$^{\Delta N}$ with CATT repeat DNA. (**A**) Various FAM labeled oligonucleotides were incubated with increasing concentrations of Pit-1$^{\Delta N}$ and anisotropy was plotted against calculated molar equivalents. Segmental linear regression for Pit-1$^{\Delta N}$/[DNA] > 1 was carried out to determine the point at which a plateau was obtained. For the 4xCATT sample, this occurred at 2.49 equivalents of Pit-1$^{\Delta N}$ to one equivalent of 4xCATT. (**B**) Gel filtration runs were carried out with Pit-1$^{\Delta N}$ and 4xCATT. At the concentration used for gel filtration experiments, relative to 4xCATT, Pit-1$^{\Delta N}$ shows negligible absorbance at 260 nm. This allows for characterization of the interaction by shifts in apparent molecular weight of the 4xCATT DNA. Apparent molecular weights are determined by calibration with standards (inset). Upon one equivalent of Pit-1$^{\Delta N}$ a doublet peak is formed. Upon titration of two equivalents of Pit-1$^{\Delta N}$ a single peak at higher molecular weight is formed. Error bars in a represent S.D. for mean from triplicate samples.

A nucleotide-residue contact map (Figure 5C) was obtained by using the DNAproDB website (43). Residues identified in the contact map have significantly buried accessible surface area, interact with bases and/or interact with backbone atoms in the DNA molecule. The primary POU_S residues mediating specific hydrogen bonding interactions with bases of the 4xCATT sequence are Gln44, Thr45 and Arg49. For the POU_H domain specifically interacting residues are Arg95, Asn141 and Gln144. To determine if the Pit-1 binding interactions on each strand were identical, the two monomers with the binding sites were overlaid (Figure 6A). The Pit-1 monomers and bases between the domains overlay perfectly, however the bases above and below the monomers show deviations, despite having identical sequences. This result clearly shows that there are asymmetric perturbations to the DNA occurring around the binding sites. A superposition of the 4xCATT complex with ideal strand B-DNA shows that the most significant perturbations occur between the two Pit-1 monomers (Figure 6B). There are no direct residue contacts between Pit-1 monomers, in the context of the DNA deformations, this in-

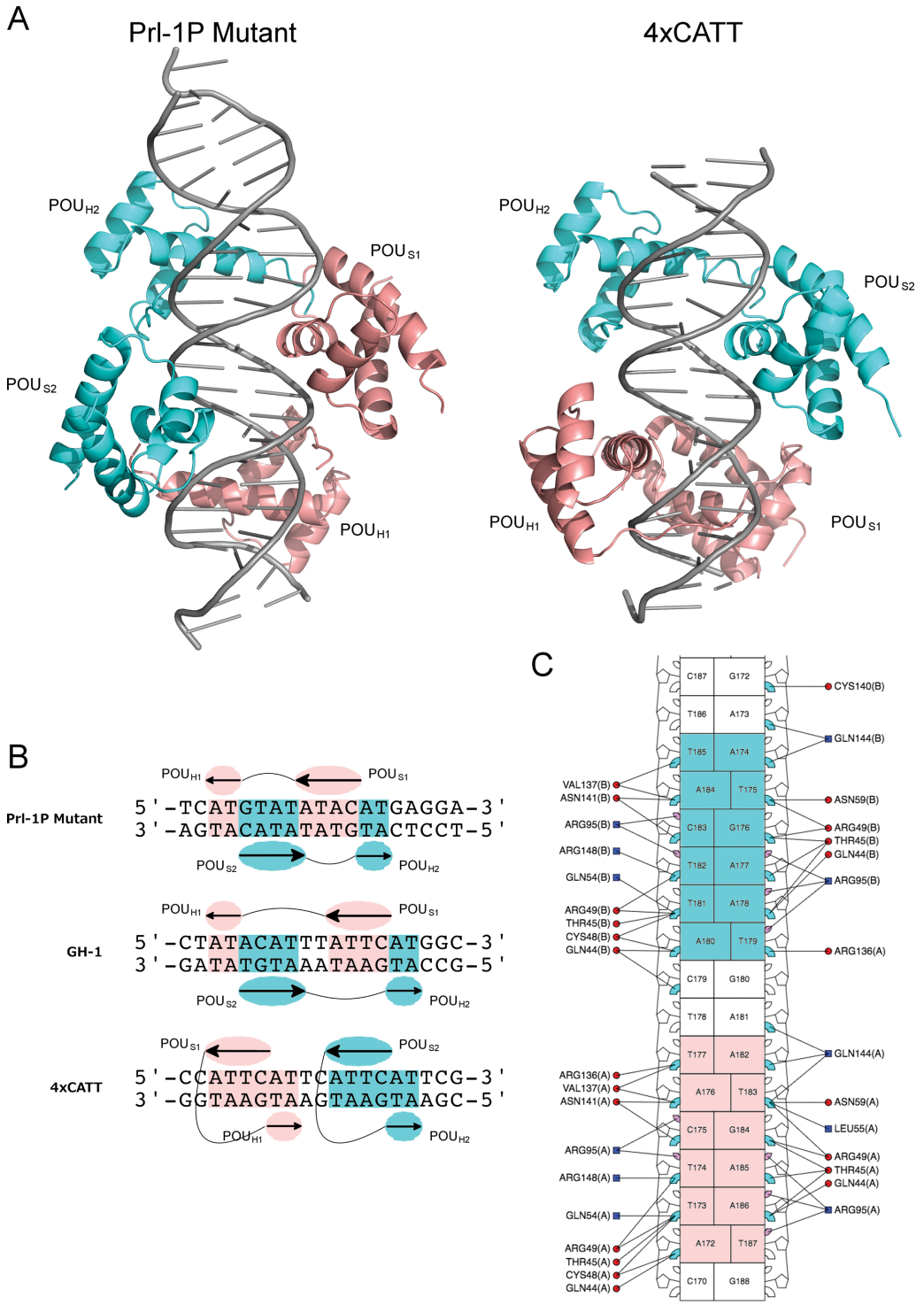

Figure 5. Structural characterization of the Pit-1/4xCATT complex with chain B in teal with chain A in salmon (figure adapted from (17)). (**A**) Structure of Pit-1 bound to the symmetric mutant Prl-1P sequence on the left and the 4xCATT sequence on the right. The Prl-1P mutant sequence was created by screening a number of different palindromic oligonucleotides with differing spacing between the Prl-1P consensus sequence (79). The 4xCATT sequence binds Pit-1 in a 2:1 molar ratio. The POU_{H2} domains bind in an identical way in both structures, surprisingly the POU_{S1} (Prl-1P) and POU_{S2} (4xCATT) sequences bind in relatively identical ways as well, resulting in a reorientation of domains. (**B**) The schematic overview of previously characterized Pit-1 complexes underscores the dramatic reorientation of domains present in the 4xCATT structure. In the 4xCATT complex structure, the two Pit-1 proteins bind identical sequences, and the sites are related by a simple rotation and translation down the DNA. Two CATT repeats encompass the binding site for each monomer. (**C**) A nucleotide residue contact map was generated using the DNAproDB website (43). Amino acid residues as part of helices are represented as red circles and as part of loop residues as blue squares. Cyan marks in the map indicate major grove contacts while pink marks represent minor grove contacts.

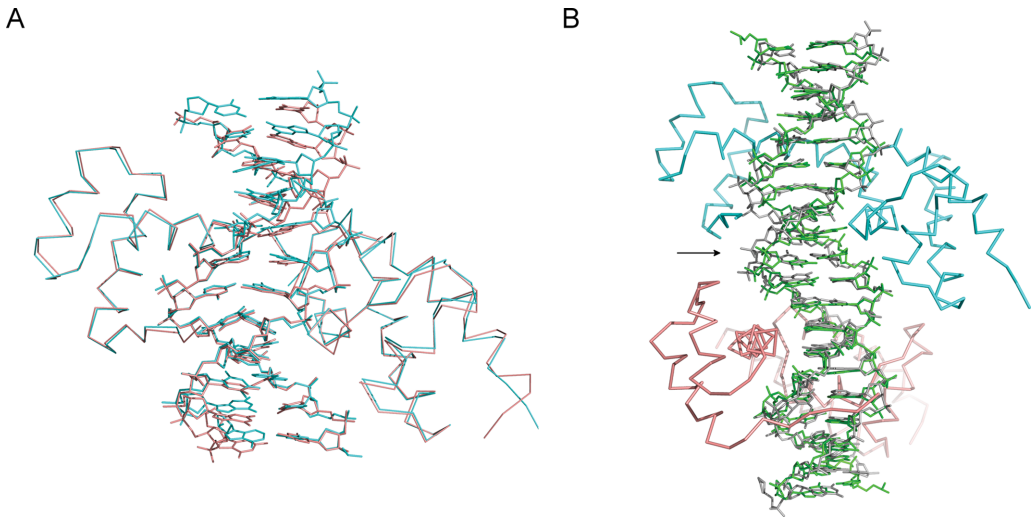

Figure 6. Structural analysis of DNA deformations (colors as in Figure 5). (**A**) Superimposition of the 2 identified Pit-1 monomers. The backbone of the Pit-1 molecules overlay well as a majority of the bases directly between the POU_S and POU_H domains, however bases located above and below the domains do not overlay as well, indicating asymmetric binding. (**B**) Overlay of an ideal B-strand DNA (green) and complex DNA (gray) with the same nucleotide sequences. The majority of deformations in the structure occur between the monomers in the region shown by the arrow.

dicates that the observed cooperativity is mediated allosterically through the DNA.

DISCUSSION

We initially investigated UHRF1 and Pit-1 for direct interactions with the *MIF* regulatory CATT microsatellite. EMSA results showed that Pit-1 shows a strong direct interaction, and that UHRF1 does not. Previously characterized interactions of Pit-1 with partner transcription factors have been shown to be dependent on the phosphorylation state of Pit-1. Phosphorylation of Pit-1 by PKA has shown increases and decreases in affinity for DNA binding, additionally effects on complex formation have been identified (19,22,23). We show that Pit-1 affinity for the CATT repeats is reduced upon phosphorylation. Further complicating this system is the ability of Pit-1 to function as both a transcriptional activator and repressor (12,17). The recent characterization of Pit-1 being upregulated in THP-1 cells as a result of stimulation with proinflammatory molecules and the identification of PKA as directly inhibiting NLRP3 inflammasome activation is consistent with unphosphorylated Pit-1 playing a proinflammatory role (13,52). However what role post translational modifications and the interaction with other transcription factors play in regulating the *MIF* promoter region have yet to be elucidated.

POU domain proteins show significant flexibility in sequence recognition. Complicating this situation is the fact that high-affinity binding sites for POU domains act cooperatively with lower affinity sites, producing dimers (18,53). The distributions of peaks from gel filtration experiments indicated a cooperative binding mechanism, consistent with previously observed behavior for Pit-1 (15). Variability of transcription factor binding as a response to different DNA sequences represents a major complication in identifying specific interactions, creating mechanistic models and predicting corresponding functional consequences (54). Pit-1 binding to the 4xCATT sequence shows an extraordinary structural rearrangement of Pit-1 domains when compared to Pit-1 binding the Prl-1P and GH-1 sequences. Similar POU domain rearrangements are dictated by the character of MORE and PORE DNA half-sites in complex with the POU transcription factor Oct-1 (55). Different resulting binding surfaces allow the Oct-1:PORE arrangement to recruit the Oct-1 specific coactivator OBF-1, while Oct-1:MORE complex is unable to complex with OBF-1 (56,57). The 4xCATT binding half sites are reminiscent of the PORE sites while the Prl-1 and GH-1 sites are similar to the MORE sites. However, the orientation of the half-sites in the 4xCATT and PORE sequences still differs, resulting in the POU domains remaining oriented differently with respect to one another (57).

The 2xCATT sequence represents the minimal sequence necessary for Pit-1 binding, however its affinity was lower than 4xCATT. This discrepancy can be explained by the clear presence of cooperativity, identified by gel filtration. Homotypic cooperativity leads to an increase in the length of the regulatory element identified, resulting in increased sequence specificity and is a common mechanism by which transcription factors specifically identify targets (58,59). Asymmetric perturbations to the DNA strand identified between the bound Pit-1 monomers supports a mechanism where the DNA allosterically mediates the cooperativity. Cooperativity between transcription factors has been identified structurally and shown to change recognized DNA sequence motifs through changes in DNA shape (59–62). In certain cases this has been shown to occur through quenching of the vibrational modes of DNA (63). Many characterized systems of gene regulation have shown protein–protein cooperative interactions with DNA that lead to significant increases in affinity ranging from 4- to 20-fold (64). Remaining variability in the IC_{50} normalized by [CATT] value for sequences greater than four repeats is likely due to a combination of changes in the stoichiometry, changes in DNA deformation effects, and resulting changes in cooperative in-

teractions. With the insight that the CATT repeat sequence results in a structurally dramatic rearrangement of the transcription factor complex, both the effects on recruitment of additional factors and the functional effects of this structural rearrangement can be explored further.

Bouckenooghe *et al.* have shown that under proinflammatory conditions, Pit-1 is upregulated in THP-1 macrophages and prolactin expression (under Pit-1 control) is concurrently increased (13). Supporting the proinflammatory role of Pit-1, prolactin is a hormone that has been established as an enhancer of immune response through upregulation of Th1 type cytokines (65,66). Given multiple pieces of evidence that Pit-1 plays an important proinflammatory role in THP-1 cells, our data characterizing the Pit-1 interaction with a region in the MIF promoter contributes to the developing importance of this transcription factor in inflammatory response. A putative SP-1 binding site in the first intron has been established to play an enhancer role in MIF transcription (6). The enhancer function of the CATT region has yet to be established, however we believe it is likely that the CATT repeat element plays a similar role. Pit-1 participates a wide number of interactions by acting as a platform to recruit co-activator/repressor complexes (67,68). UHRF1 as a multidomain protein, broadly regulates gene expression and plays a central role in regulatory events in the cell (69). UHRF1 is able to integrate a wide variety of information from cellular signals including ubiquitination, hemi-methylated CpG DNA, histone acetylation and phosphatidylinositols (70,71). In addition, UHRF1 has been shown to interact with a number of different proteins, including histones (72), DNMT1 (71,73) and BRCA1 (69). In context of the previously characterized roles of Pit-1 and UHRF1, their identification in interactions with the MIF promoter (11) and our work here, we hypothesize that they may form a complex reminiscent of the PORE/Oct-1/OBF-1 complex to control MIF transcription.

We find the mechanism of Pit-1 binding to target DNA is highly dependent on oligonucleotide sequence. In the context of the cell, the ultimate functional effect of Pit-1 binding is extraordinarily dependent on both sequence and genomic context, where histones and other co-repressor/activator proteins play a major role in gene regulation outcomes (12,17). Additional *in vivo* functional experiments will need to be carried out to determine the effect of the variables studied in this paper on expression of MIF. Our work broadly underscores the amazing versatility with which transcription factors can specifically identify target sequences and the critical role cooperativity plays in specifically binding target sequences. More specifically we shed light on the mechanism by which Pit-1 interacts with the CATT repeats and lay the groundwork for further investigations of the functionally important microsatellite region. Characterization of interactions between Pit-1, DNA and putative interacting transcription factors like UHRF1 will be needed for a complete understanding of this system. The fluorescence anisotropy assays developed here can be used to characterize the interactions of putative co-factors and to screen for drug candidates in hopes of developing more effective therapeutic treatments for a wide variety of MIF mediated diseases.

AVAILABILITY

Atomic coordinates and structure factors for the reported crystal structure have been deposited with the Protein Data bank under accession number 5WC9.

SUPPLEMENTARY DATA

Supplementary Data are available at NAR online.

ACKNOWLEDGEMENTS

We thank Alessandro Vindigni for helpful comments on the manuscript and Sergey Korolev for his help in characterizing the structure.

FUNDING

Saint Louis University. Funding for open access charge: Saint Louis University.
Conflict of interest statement. None declared.

REFERENCES

1. Calandra,T. and Roger,T. (2003) Macrophage migration inhibitory factor: a regulator of innate immunity. *Nat. Rev. Immunol.*, **3**, 791–800.
2. Bacher,M., Metz,C.N., Calandra,T., Mayer,K., Chesney,J., Lohoff,M., Gemsa,D., Donnelly,T. and Bucala,R. (1996) An essential regulatory role for macrophage migration inhibitory factor in T-cell activation. *Proc. Natl. Acad. Sci. U.S.A.*, **93**, 7849–7854.
3. Calandra,T., Echtenacher,B., Roy,D.L., Pugin,J., Metz,C.N., Hultner,L., Heumann,D., Mannel,D., Bucala,R. and Glauser,M.P. (2000) Protection from septic shock by neutralization of macrophage migration inhibitory factor. *Nat. Med.*, **6**, 164–170.
4. Calandra,T., Froidevaux,C., Martin,C. and Roger,T. (2003) Macrophage migration inhibitory factor and host innate immune defenses against bacterial sepsis. *J. Infect. Dis.*, **187**, S385–S390.
5. Nishihira,J. and Mitsuyama,K. (2009) Overview of the role of macrophage migration inhibitory factor (MIF) in inflammatory bowel disease. *Curr. Pharm. Des.*, **15**, 2104–2109.
6. Beaulieu,E., Green,L., Elsby,L., Alourfi,Z., Morand,E.F., Ray,D.W. and Donn,R. (2011) Identification of a novel cell type-specific intronic enhancer of macrophage migration inhibitory factor (MIF) and its regulation by mithramycin. *Clin. Exp. Immunol.*, **163**, 178–188.
7. Welford,S.M., Bedogni,B., Gradin,K., Poellinger,L., Broome Powell,M. and Giaccia,A.J. (2006) HIF1alpha delays premature senescence through the activation of MIF. *Genes Dev.*, **20**, 3366–3371.
8. Baugh,J.A., Gantier,M., Li,L., Byrne,A., Buckley,A. and Donnelly,S.C. (2006) Dual regulation of macrophage migration inhibitory factor (MIF) expression in hypoxia by CREB and HIF-1. *Biochem. Biophys. Res. Commun.*, **347**, 895–903.
9. Baugh,J.A., Chitnis,S., Donnelly,S.C., Monteiro,J., Lin,X., Plant,B.J., Wolfe,F., Gregersen,P.K. and Bucala,R. (2002) A functional promoter polymorphism in the macrophage migration inhibitory factor (MIF) gene associated with disease severity in rheumatoid arthritis. *Genes Immun.*, **3**, 170–176.
10. Barton,A., Lamb,R., Symmons,D., Silman,A., Thomson,W., Worthington,J. and Donn,R. (2003) Macrophage migration inhibitory factor (MIF) gene polymorphism is associated with susceptibility to but not severity of inflammatory polyarthritis. *Genes Immun.*, **4**, 487–491.
11. Yao,J., Leng,L., Sauler,M., Fu,W., Zheng,J., Zhang,Y., Du,X., Yu,X., Lee,P. and Bucala,R. (2016) Transcription factor ICBP90 regulates the MIF promoter and immune susceptibility locus. *J. Clin. Invest.*, **126**, 732–744.
12. Kashiwabara,Y., Sasaki,S., Matsushita,A., Nagayama,K., Ohba,K., Iwaki,H., Matsunaga,H., Suzuki,S., Misawa,H., Ishizuka,K. *et al.* (2009) Functions of PIT1 in GATA2-dependent transactivation of the thyrotropin beta promoter. *J. Mol. Endocrinol.*, **42**, 225–237.

13. Bouckenooghe,T., Sisino,G., Aurientis,S., Chinetti-Gbaguidi,G., Kerr-Conte,J., Staels,B., Fontaine,P., Storme,L., Pattou,F. and Vambergue,A. (2014) Adipose tissue macrophages (ATM) of obese patients are releasing increased levels of prolactin during an inflammatory challenge: a role for prolactin in diabesity? *Biochim. Biophys. Acta*, **1842**, 584–593.
14. Seoane,S., Arias,E., Sigueiro,R., Sendon-Lago,J., Martinez-Ordonez,A., Castelao,E., Eiro,N., Garcia-Caballero,T., Macia,M., Lopez-Lopez,R. *et al.* (2015) Pit-1 inhibits BRCA1 and sensitizes human breast tumors to cisplatin and vitamin D treatment. *Oncotarget*, **6**, 14456–14471.
15. Ingraham,H.A., Flynn,S.E., Voss,J.W., Albert,V.R., Kapiloff,M.S., Wilson,L. and Rosenfeld,M.G. (1990) The POU-specific domain of Pit-1 is essential for sequence-specific, high affinity DNA binding and DNA-dependent Pit-1-Pit-1 interactions. *Cell*, **61**, 1021–1033.
16. Xu,L., Lavinsky,R.M., Dasen,J.S., Flynn,S.E., McInerney,E.M., Mullen,T.M., Heinzel,T., Szeto,D., Korzus,E., Kurokawa,R. *et al.* (1998) Signal-specific co-activator domain requirements for Pit-1 activation. *Nature*, **395**, 301–306.
17. Scully,K.M., Jacobson,E.M., Jepsen,K., Lunyak,V., Viadiu,H., Carriere,C., Rose,D.W., Hooshmand,F., Aggarwal,A.K. and Rosenfeld,M.G. (2000) Allosteric effects of Pit-1 DNA sites on long-term repression in cell type specification. *Science*, **290**, 1127–1131.
18. Andersen,B. and Rosenfeld,M.G. (2001) POU domain factors in the neuroendocrine system: lessons from developmental biology provide insights into human disease. *Endocr. Rev.*, **22**, 2–35.
19. Augustijn,K.D., Duval,D.L., Wechselberger,R., Kaptein,R., Gutierrez-Hartmann,A. and van der Vliet,P.C. (2002) Structural characterization of the PIT-1/ETS-1 interaction: PIT-1 phosphorylation regulates PIT-1/ETS-1 binding. *Proc. Natl. Acad. Sci. U.S.A.*, **99**, 12657–12662.
20. Voss,J.W., Wilson,L. and Rosenfeld,M.G. (1991) POU-domain proteins Pit-1 and Oct-1 interact to form a heteromeric complex and can cooperate to induce expression of the prolactin promoter. *Genes Dev.*, **5**, 1309–1320.
21. Shewchuk,B.M., Ho,Y., Liebhaber,S.A. and Cooke,N.E. (2006) A single base difference between Pit-1 binding sites at the hGH promoter and locus control region specifies distinct Pit-1 conformations and functions. *Mol. Cell. Biol.*, **26**, 6535–6546.
22. Kapiloff,M.S., Farkash,Y., Wegner,M. and Rosenfeld,M.G. (1991) Variable effects of phosphorylation of Pit-1 dictated by the DNA response elements. *Science*, **253**, 786–789.
23. Steinfelder,H.J., Radovick,S. and Wondisford,F.E. (1992) Hormonal regulation of the thyrotropin beta-subunit gene by phosphorylation of the pituitary-specific transcription factor Pit-1. *Proc. Natl. Acad. Sci. U.S.A.*, **89**, 5942–5945.
24. Jean,A., Gutierrez-Hartmann,A. and Duval,D.L. (2010) A Pit-1 threonine 220 phosphomimic reduces binding to monomeric DNA sites to inhibit Ras and estrogen stimulation of the prolactin gene promoter. *Mol. Endocrinol.*, **24**, 91–103.
25. Kapust,R.B., Tozser,J., Fox,J.D., Anderson,D.E., Cherry,S., Copeland,T.D. and Waugh,D.S. (2001) Tobacco etch virus protease: mechanism of autolysis and rational design of stable mutants with wild-type catalytic proficiency. *Protein Eng.*, **14**, 993–1000.
26. Narayana,N., Cox,S., Shaltiel,S., Taylor,S.S. and Xuong,N. (1997) Crystal structure of a polyhistidine-tagged recombinant catalytic subunit of cAMP-dependent protein kinase complexed with the peptide inhibitor PKI(5-24) and adenosine. *Biochemistry*, **36**, 4438–4448.
27. Seiler,C.Y., Park,J.G., Sharma,A., Hunter,P., Surapaneni,P., Sedillo,C., Field,J., Algar,R., Price,A., Steel,J. *et al.* (2014) DNASU plasmid and PSI:Biology-Materials repositories: resources to accelerate biological research. *Nucleic Acids Res.*, **42**, D1253–D1260.
28. Sidorova,N.Y., Hung,S. and Rau,D.C. (2010) Stabilizing labile DNA-protein complexes in polyacrylamide gels. *Electrophoresis*, **31**, 648–653.
29. Hellman,L.M. and Fried,M.G. (2007) Electrophoretic mobility shift assay (EMSA) for detecting protein-nucleic acid interactions. *Nat. Protoc.*, **2**, 1849–1861.
30. Prinz,H. (2010) Hill coefficients, dose-response curves and allosteric mechanisms. *J. Chem. Biol.*, **3**, 37–44.
31. Mendel,C.M. and Mendel,D.B. (1985) 'Non-specific' binding. The problem, and a solution. *Biochem. J.*, **228**, 269–272.
32. Ni,L., Xu,W., Kumaraswami,M. and Schumacher,M.A. (2010) Plasmid protein TubR uses a distinct mode of HTH-DNA binding and recruits the prokaryotic tubulin homolog TubZ to effect DNA partition. *Proc. Natl. Acad. Sci. U.S.A.*, **107**, 11763–11768.
33. Arosio,D., Costantini,S., Kong,Y. and Vindigni,A. (2004) Fluorescence anisotropy studies on the Ku-DNA interaction: anion and cation effects. *J. Biol. Chem.*, **279**, 42826–42835.
34. Battye,T.G., Kontogiannis,L., Johnson,O., Powell,H.R. and Leslie,A.G. (2011) iMOSFLM: a new graphical interface for diffraction-image processing with MOSFLM. *Acta Crystallogr. D Biol. Crystallogr.*, **67**, 271–281.
35. Foadi,J., Aller,P., Alguel,Y., Cameron,A., Axford,D., Owen,R.L., Armour,W., Waterman,D.G., Iwata,S. and Evans,G. (2013) Clustering procedures for the optimal selection of data sets from multiple crystals in macromolecular crystallography. *Acta Crystallogr. D Biol. Crystallogr.*, **69**, 1617–1632.
36. Winn,M.D., Ballard,C.C., Cowtan,K.D., Dodson,E.J., Emsley,P., Evans,P.R., Keegan,R.M., Krissinel,E.B., Leslie,A.G., McCoy,A. *et al.* (2011) Overview of the CCP4 suite and current developments. *Acta Crystallogr. D Biol. Crystallogr.*, **67**, 235–242.
37. Evans,P.R. (2011) An introduction to data reduction: space-group determination, scaling and intensity statistics. *Acta Crystallogr. D Biol. Crystallogr.*, **67**, 282–292.
38. Evans,P.R. and Murshudov,G.N. (2013) How good are my data and what is the resolution? *Acta Crystallogr. D Biol. Crystallogr.*, **69**, 1204–1214.
39. Adams,P.D., Afonine,P.V., Bunkoczi,G., Chen,V.B., Davis,I.W., Echols,N., Headd,J.J., Hung,L.W., Kapral,G.J., Grosse-Kunstleve,R.W. *et al.* (2010) PHENIX: a comprehensive Python-based system for macromolecular structure solution. *Acta Crystallogr. D Biol. Crystallogr.*, **66**, 213–221.
40. Chen,V.B., Arendall,W.B. 3rd, Headd,J.J., Keedy,D.A., Immormino,R.M., Kapral,G.J., Murray,L.W., Richardson,J.S. and Richardson,D.C. (2010) MolProbity: all-atom structure validation for macromolecular crystallography. *Acta Crystallogr. D Biol. Crystallogr.*, **66**, 12–21.
41. Schrodinger, LLC (2015) https://www.schrodinger.com/.
42. Morin,A., Eisenbraun,B., Key,J., Sanschagrin,P.C., Timony,M.A., Ottaviano,M. and Sliz,P. (2013) Collaboration gets the most out of software. *Elife*, **2**, e01456.
43. Sagendorf,J.M., Berman,H.M. and Rohs,R. (2017) DNAproDB: an interactive tool for structural analysis of DNA-protein complexes. *Nucleic Acids Res.*, **45**, W89–W97.
44. Trotzier,M.A., Bronner,C., Bathami,K., Mathieu,E., Abbady,A.Q., Jeanblanc,M., Muller,C.D., Rochette-Egly,C. and Mousli,M. (2004) Phosphorylation of ICBP90 by protein kinase A enhances topoisomerase IIalpha expression. *Biochem. Biophys. Res. Commun.*, **319**, 590–595.
45. Sobrier,M.L., Tsai,Y.C., Perez,C., Leheup,B., Bouceba,T., Duquesnoy,P., Copin,B., Sizova,D., Penzo,A., Stanger,B.Z. *et al.* (2016) Functional characterization of a human POU1F1 mutation associated with isolated growth hormone deficiency: a novel etiology for IGHD. *Hum. Mol. Genet.*, **25**, 472–483.
46. Cann,J.R. (1989) Phenomenological theory of gel electrophoresis of protein-nucleic acid complexes. *J. Biol. Chem.*, **264**, 17032–17040.
47. Rossi,A.M. and Taylor,C.W. (2011) Analysis of protein-ligand interactions by fluorescence polarization. *Nat. Protoc.*, **6**, 365–387.
48. Cheng,Y. and Prusoff,W.H. (1973) Relationship between the inhibition constant (K1) and the concentration of inhibitor which causes 50 per cent inhibition (I50) of an enzymatic reaction. *Biochem. Pharmacol.*, **22**, 3099–3108.
49. Jacobson,E.M., Li,P., Leon-del-Rio,A., Rosenfeld,M.G. and Aggarwal,A.K. (1997) Structure of Pit-1 POU domain bound to DNA as a dimer: unexpected arrangement and flexibility. *Genes Dev.*, **11**, 198–212.
50. Chojnowski,G. and Bochtler,M. (2010) DIBER: protein, DNA or both? *Acta Crystallogr. D Biol. Crystallogr.*, **66**, 643–653.
51. Girard,E., Prange,T., Dhaussy,A.C., Migianu-Griffoni,E., Lecouvey,M., Chervin,J.C., Mezouar,M., Kahn,R. and Fourme,R. (2007) Adaptation of the base-paired double-helix molecular architecture to extreme pressure. *Nucleic Acids Res.*, **35**, 4800–4808.
52. Mortimer,L., Moreau,F., MacDonald,J.A. and Chadee,K. (2016) NLRP3 inflammasome inhibition is disrupted in a group of

auto-inflammatory disease CAPS mutations. *Nat. Immunol.*, **17**, 1176–1186.
53. Howard,P.W. and Maurer,R.A. (1995) A composite Ets/Pit-1 binding site in the prolactin gene can mediate transcriptional responses to multiple signal transduction pathways. *J. Biol. Chem.*, **270**, 20930–20936.
54. Siggers,T. and Gordan,R. (2014) Protein-DNA binding: complexities and multi-protein codes. *Nucleic Acids Res.*, **42**, 2099–2111.
55. Tomilin,A., Remenyi,A., Lins,K., Bak,H., Leidel,S., Vriend,G., Wilmanns,M. and Scholer,H.R. (2000) Synergism with the coactivator OBF-1 (OCA-B, BOB-1) is mediated by a specific POU dimer configuration. *Cell*, **103**, 853–864.
56. Remenyi,A., Tomilin,A., Scholer,H.R. and Wilmanns,M. (2002) Differential activity by DNA-induced quarternary structures of POU transcription factors. *Biochem. Pharmacol.*, **64**, 979–984.
57. Remenyi,A., Tomilin,A., Pohl,E., Lins,K., Philippsen,A., Reinbold,R., Scholer,H.R. and Wilmanns,M. (2001) Differential dimer activities of the transcription factor Oct-1 by DNA-induced interface swapping. *Mol Cell*, **8**, 569–580.
58. Todeschini,A.L., Georges,A. and Veitia,R.A. (2014) Transcription factors: specific DNA binding and specific gene regulation. *Trends Genet.*, **30**, 211–219.
59. Morgunova,E. and Taipale,J. (2017) Structural perspective of cooperative transcription factor binding. *Curr. Opin. Struct. Biol.*, **47**, 1–8.
60. Panne,D. (2008) The enhanceosome. *Curr. Opin. Struct. Biol.*, **18**, 236–242.
61. Luna-Zurita,L., Stirnimann,C.U., Glatt,S., Kaynak,B.L., Thomas,S., Baudin,F., Samee,M.A., He,D., Small,E.M., Mileikovsky,M. *et al.* (2016) Complex interdependence regulates heterotypic transcription factor distribution and coordinates cardiogenesis. *Cell*, **164**, 999–1014.
62. Shiina,M., Hamada,K., Inoue-Bungo,T., Shimamura,M., Uchiyama,A., Baba,S., Sato,K., Yamamoto,M. and Ogata,K. (2015) A novel allosteric mechanism on protein-DNA interactions underlying the phosphorylation-dependent regulation of Ets1 target gene expressions. *J. Mol. Biol.*, **427**, 1655–1669.
63. Kim,S., Brostromer,E., Xing,D., Jin,J., Chong,S., Ge,H., Wang,S., Gu,C., Yang,L., Gao,Y.Q. *et al.* (2013) Probing allostery through DNA. *Science*, **339**, 816–819.
64. Polach,K.J. and Widom,J. (1996) A model for the cooperative binding of eukaryotic regulatory proteins to nucleosomal target sites. *J. Mol. Biol.*, **258**, 800–812.
65. Peeva,E. and Zouali,M. (2005) Spotlight on the role of hormonal factors in the emergence of autoreactive B-lymphocytes. *Immunol. Lett.*, **101**, 123–143.
66. Matera,L. and Mori,M. (2000) Cooperation of pituitary hormone prolactin with interleukin-2 and interleukin-12 on production of interferon-gamma by natural killer and T cells. *Ann. N. Y. Acad. Sci.*, **917**, 505–513.
67. Phillips,K. and Luisi,B. (2000) The virtuoso of versatility: POU proteins that flex to fit. *J. Mol. Biol.*, **302**, 1023–1039.
68. Cohen,R.N., Brue,T., Naik,K., Houlihan,C.A., Wondisford,F.E. and Radovick,S. (2006) The role of CBP/p300 interactions and Pit-1 dimerization in the pathophysiological mechanism of combined pituitary hormone deficiency. *J. Clin. Endocrinol. Metab.*, **91**, 239–247.
69. Zhang,H., Liu,H., Chen,Y., Yang,X., Wang,P., Liu,T., Deng,M., Qin,B., Correia,C., Lee,S. *et al.* (2016) A cell cycle-dependent BRCA1-UHRF1 cascade regulates DNA double-strand break repair pathway choice. *Nat. Commun.*, **7**, 10201.
70. Gelato,K.A., Tauber,M., Ong,M.S., Winter,S., Hiragami-Hamada,K., Sindlinger,J., Lemak,A., Bultsma,Y., Houliston,S., Schwarzer,D. *et al.* (2014) Accessibility of different histone H3-binding domains of UHRF1 is allosterically regulated by phosphatidylinositol 5-phosphate. *Mol. Cell*, **54**, 905–919.
71. Fang,J., Cheng,J., Wang,J., Zhang,Q., Liu,M., Gong,R., Wang,P., Zhang,X., Feng,Y., Lan,W. *et al.* (2016) Hemi-methylated DNA opens a closed conformation of UHRF1 to facilitate its histone recognition. *Nat. Commun.*, **7**, 11197.
72. Arita,K., Isogai,S., Oda,T., Unoki,M., Sugita,K., Sekiyama,N., Kuwata,K., Hamamoto,R., Tochio,H., Sato,M. *et al.* (2012) Recognition of modification status on a histone H3 tail by linked histone reader modules of the epigenetic regulator UHRF1. *Proc. Natl. Acad. Sci. U.S.A.*, **109**, 12950–12955.
73. Bostick,M., Kim,J.K., Esteve,P.O., Clark,A., Pradhan,S. and Jacobsen,S.E. (2007) UHRF1 plays a role in maintaining DNA methylation in mammalian cells. *Science*, **317**, 1760–1764.
74. Daily,K., Patel,V.R., Rigor,P., Xie,X. and Baldi,P. (2011) MotifMap: integrative genome-wide maps of regulatory motif sites for model species. *BMC Bioinformatics*, **12**, 495.
75. Dambacher,J., Staudinger,T., Seiderer,J., Sisic,Z., Schnitzler,F., Pfennig,S., Hofbauer,K., Konrad,A., Tillack,C., Otte,J.M. *et al.* (2007) Macrophage migration inhibitory factor (MIF) -173G/C promoter polymorphism influences upper gastrointestinal tract involvement and disease activity in patients with Crohn's disease. *Inflamm. Bowel Dis.*, **13**, 71–82.
76. Donn,R.P., Shelley,E., Ollier,W.E., Thomson,W. and British Paediatric Rheumatology Study, G. (2001) A novel 5'-flanking region polymorphism of macrophage migration inhibitory factor is associated with systemic-onset juvenile idiopathic arthritis. *Arthritis Rheum*, **44**, 1782–1785.
77. Buchan,D.W., Minneci,F., Nugent,T.C., Bryson,K. and Jones,D.T. (2013) Scalable web services for the PSIPRED Protein Analysis Workbench. *Nucleic Acids Res.*, **41**, W349–W357.
78. Robert,X. and Gouet,P. (2014) Deciphering key features in protein structures with the new ENDscript server. *Nucleic Acids Res.*, **42**, W320–W324.
79. Jacobson,E.M., Li,P., Rosenfeld,M.G. and Aggarwal,A.K. (1996) Crystallization and preliminary X-ray analysis of Pit-1 POU domain complexed to a 28 base pair DNA element. *Proteins*, **24**, 263–265.